THE THREE GENERATIONS OF GOLD IN THE PALAI–ISLICA EPITHERMAL DEPOSIT, SOUTHEASTERN SPAIN

F. Javier CARRILLO ROSÚA, Salvador MORALES RUANO[§] and Puri FENOLL HACH-ALÍ

Instituto Andaluz de Ciencias de la Tierra (*CSIC–UGR*) *and Department of Mineralogy and Petrology,
University of Granada, Avda. Fuentenueva s/n, E–18002 Granada, Spain*

ABSTRACT

In the Palai–Islica deposit, in southeastern Spain, gold is found associated with sulfide mineralization (particularly Fe sulfides). Grains of Au–Ag alloy (gold of types A and B) occur with pyrite in mineralized veins, and grains of native gold (type C) are associated with areas of massive silicification at the uppermost levels of the deposit. The content of "invisible" gold in the various Fe sulfides is practically nil. Of all the textural varieties of pyrite studied, unzoned medium- to coarse-grained pyrite is the only one bearing gold. A clear distinction can be established between three types of gold (A, B and C), each with a different genesis. Grains of type-A alloy deposited as a result of variations in the thermodynamic parameters of the system, mainly a decrease in sulfur activity, whereas the appearance of the type-B alloy was mainly controlled by electrochemical factors. Type-C gold may have been produced from colloidal solutions in significantly different geochemical conditions. The chemical evolution of the alloys is characterized by Ag enrichment as precipitation continued. Type-A grains [mean Au/(Au + Ag) = 0.861] were the first to form, encased in the pyrite, with a relatively low Ag content and barely any zonation, followed by gold of type B, overgrowing pyrite, with a higher average Ag content [Au/(Au + Ag) = 0.756] and commonly zoned, with later zones richer in Ag. Finally, type-C native gold has practically no Ag [on average, Au/(Au + Ag) = 0.988].

Keywords: gold, gold–silver alloy, epithermal deposit, Palai–Islica, Spain.

SOMMAIRE

Dans le gisement de Palai–Islica, de la partie sud-est de l'Espagne, l'or est associé avec la minéralisation en sulfures, de fer surtout. Les grains d'un alliage Au–Ag (or de types A et B) sont associés à la pyrite dans les veines minéralisées, et les grains d'or natif (dits de type C) sont associés aux zones de silicification massive dans les parties supérieures du gisement. La teneur en or "invisible" des divers sulfures de fer est quasiment nulle. De toutes les variétés texturales de pyrite étudiées, seule la génération de pyrite en grains non zonés et à granulométrie moyenne à grossière est aurifère. On peut établir une distinction nette entre les trois types d'or (A, B et C), chacune ayant une différente genèse. Les grains d'alliage de type A ont été déposés suite à des variations des paramètres thermodynamiques du système, surtout une diminution de l'activité du soufre, tandis que la formation des grains d'alliage de type B était surtout régie par des facteurs électrochimiques. L'or de type C pourrait avoir été produit à partir d'une solution colloïdale dans des conditions géochimiques nettement différentes. L'évolution de l'alliage Au–Ag est marquée par un enrichissement en Ag au fur et à mesure que la précipitation progressait. Les grains de type A [en moyenne, Au/(Au + Ag) = 0.861] ont été les premiers à se former, étant encastrés dans la pyrite, avec une teneur relativement faible en Ag, sans zonation importante, et ont été suivis par les grains de type B, en surcroissance de la pyrite, avec une teneur plus élevée en Ag et généralement zonés, les zones tardives étant enrichies en Ag [en moyenne, Au/(Au + Ag) = 0.756]. Finalement, l'or natif de type C ne contient à peu près pas d'argent [en moyenne, Au/(Au + Ag) = 0.988].

(Traduit par la Rédaction)

Mots-clés: or, alliage or–argent, gisement épithermal, Palai–Islica, Espagne.

[§]   *E-mail address*: smorales@ugr.es

INTRODUCTION

A large number of polymetallic hydrothermal deposits containing varying proportions of gold, silver and related metals, such as Fe–Zn–Cu–Bi–Hg–Pb–As–Sb–Sn–Ba–REE–Te, have been exploited since ancient times in the Cabo de Gata – Cartagena volcanic belt in southeastern Spain (*e.g.*, Arribas & Tosdal 1994, Morales *et al.* 2000, and references therein). These hydrothermal deposits range from epithermal to mesothermal in character and vary enormously in their host rocks, types of alteration, mineral associations, textures, paragenetic sequences and proportions of precious metals. This variability makes it difficult to establish general criteria for exploration. Nevertheless, mining activity in the region is currently increasing, and at the Palai–Islica deposit, horizons of (Au–Cu)-bearing sulfide have been demonstrated to contain economically important gold minerals.

In an earlier study, Morales *et al.* (2000) showed the presence of visible grains of gold distributed in four subhorizontal zones, the most important being called "upper geochemical anomaly, UGA" and "lower geochemical anomaly, LGA" located about 45 m and –75 m above sea level, respectively. These zones have significant geochemical anomalies in Au (up to 21 ppm), Ag (up to 110 ppm) and other metallic elements (Cu, Zn, Pb, Bi, As, Sb and Cd). Morales *et al.* (2000) also demonstrated the existence of fluids with distinct characteristics compared to those in the remainder of the deposit in these subhorizontal zones. A fluid with low salinity (mainly between 3 and 10 wt.% NaCl eq.) and high variation of temperature (between 125 and 450°C) is found over all the deposit, whereas associated with the geochemical anomalies, there is also another fluid characterized by high variation in salinity (between 2.0 and 29.3 wt.% NaCl eq.) over a temperature range of 25–50°C located between 200 and 300°C. Carrillo *et al.* (2001a) also showed the existence of a greater diversity of minerals associated with these geochemical anomalies.

Our aim in this paper is to characterize the different mineralogical and chemical expressions of gold. From an economic point of view, it is especially important to know the textural relationship between the grains of gold and the host mineral phases in order to obtain the best recovery of gold. In the same way, an estimation of gold concentration in pyrite (the most abundant sulfide phase at Palai–Islica) is very important in an evaluation of gold potential. Another of our objectives is to determine the possible mechanisms leading to concentration and precipitation of Au in this type of deposit. There are currently several ways to explain the accumulation of gold. A thermodynamic approach allows a study of the complexes having the capacity to transport gold (mainly sulfide or chloride complexes, *i.e.*, Arribas 1995), and their solubility and stability according to several thermodynamic parameters. Another approach is centered on surface processes: sorption (Renders & Seward 1989, Schoonen *et al.* 1992), reductive precipitation (Jean & Bancroft 1985, Hayland & Bancroft 1989, Knipe *et al.* 1992) and electrochemical precipitation (Moller & Kersten 1994). In the present paper, we consider these hypotheses to explain the deposition of gold in the Palai–Islica deposit.

GEOLOGICAL CONTEXT

The Cabo de Gata – Cartagena volcanic belt comprises part of the eastern end of the Internal Zone of the Betic Cordillera (Fig. 1A), which consists of three main tectonostratigraphic complexes [in ascending order: Nevado–Filabride, Alpujarride and Malaguide (Egeler & Simon 1969)]. This Neogene volcanic belt was formed within the context of a subduction zone, followed by an extensional event (Dewey 1988, García Dueñas *et al.* 1992), with very high rates of cooling and uplift (Zeck *et al.* 1992). The diversity of volcanic rocks in a relatively small area and with marked spatial distribution (from south to north) is noteworthy: calc-alkaline, potassic calc-alkaline, shoshonitic, ultrapotassic and basaltic series (Fig. 1A). In the north of Africa, separated from the Cabo de Gata – Cartagena volcanic belt by the Alboran Sea, it is also possible to find equivalent volcanic rocks (*i.e.*, Hernandez & Bellon 1985), and, on the floor of the Alboran Sea, samples of the same volcanic rocks have been collected (Comas *et al.* 1999). The calc-alkaline magmatism shows much greater volumetric development than the other series, and is the only one that hosts gold deposits: Rodalquilar (Arribas *et al.* 1995), Los Alemanes Nuevos (Pineda 1984, Demoustier *et al.* 1998) and Palai–Islica (Morales *et al.* 1999, 2000). The volcanic rocks vary from basaltic andesite to rhyolite with a medium to high K content (Fernández Soler 1996), their ages ranging from 20.9 to 7.5 m.y. (Scotney *et al.* 2000, Di Battistini *et al.* 1987).

FIG. 1. A. Location of the most important ore deposits at Cabo de Gata – Cartagena volcanic belt (from Morales *et al.* 2000). (A) calc-alkaline volcanism, (B) calc-alkaline, potassic and shoshonitic volcanism, (C) ultrapotassic volcanism, (D) basaltic volcanism. (1) Cabo de Gata and Los Alemanes Nuevos, (2) Rodalquilar, (3) Carboneras (Palai–Islica), (4) Herrerías, (5) Sierra Almagrera, (6) Aguilas), and (7) Mazarrón. B. Schematic geological map showing the location of Palai–Islica deposit (from Morales *et al.* 2000). Main geological units: (1) Upper Miocene volcanic rocks of the Cabo de Gata calc-alkaline series, (2) Paleozoic–Mesozoic basement rocks belonging to the Nevado–Filabride, Alpujarride and Malaguide complexes, (3) Tertiary sedimentary rocks, (4) Quaternary sediments, (a) alluvial and (c) colluvial, (5) faults are outlined in continuous line, and the limit of hydrothermal alteration is outlined in a dashed line, (6) the outcropping Palai–Islica deposit.
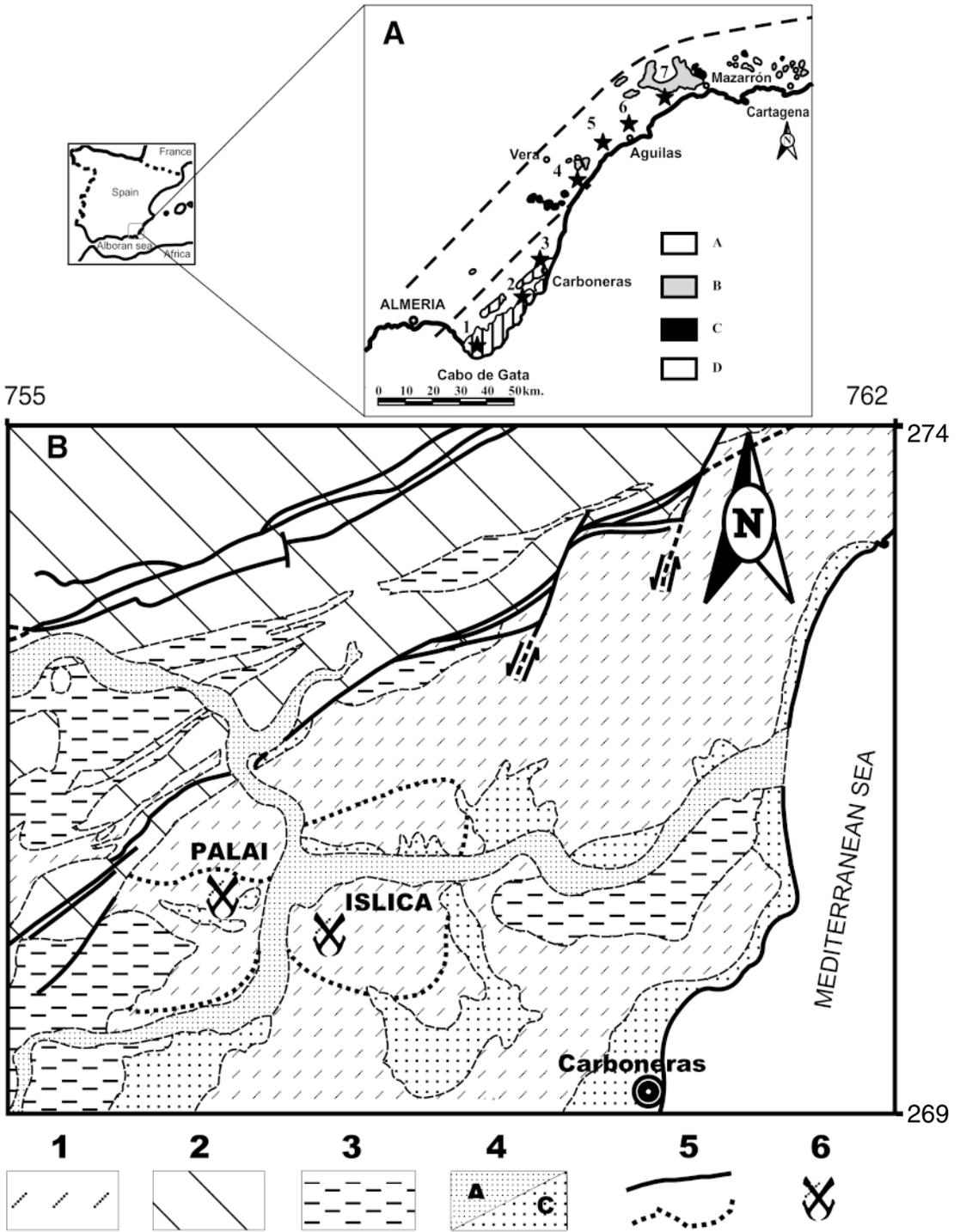
A series of hydrothermal systems developed during the Miocene in association with the various series of volcanic rocks and the system of faults and fractures controlling it (López Ruiz & Rodríguez Badiola 1980). The hot fluids [up to 400–450°C, as documented by fluid-inclusion data (Morales (1994)] reacted strongly with the host rocks and thus in some districts gave rise to the formation of broad areas of mineralization and alteration, usually zoned (Fernández Soler 1996).

One of the most important examples of these processes is the case of Au–Cu mineralization (Fig. 1B) hosted directly within the strongly hydrothermally altered calc-alkaline volcanic rocks of Carboneras (Morales *et al.* 1999, 2000). The volcanic rocks are hosted by Paleozoic and Mesozoic rocks from the Nevado–Filabride (black schists) and Alpujarride–Malaguide (phyllite, quartzite, dolomite and gypsum) complexes. Overlying the metamorphic rocks, there are also Tertiary and Quaternary materials (marl, limestone, calcarenite and alluvial and colluvial sediments). Neither basement nor overlying rocks seem to be mineralized. The Palai–Islica area (Fig. 1B) consists of an oval E–W-striking zone 2.5 km long by 1.7 km wide consisting of strongly hydrothermally altered andesite and dacite autobreccias emplaced 10.4 m.y ago (Bellon *et al*. 1983) in a domal structure (Fernandez Soler 1996). Gold-bearing mineralization is invariably related to zones of hydrothermal alteration; propylitic, sericitic, advanced argillic zones have been recognized, accompanied by silicification.

SAMPLES AND ANALYTICAL TECHNIQUES

Samples for this study were chosen from different parts of the Palai–Islica deposit in order to cover high-grade gold mineralization and zones barren of mineralization. Two hundred and twenty-two polished thin-sections of samples collected from 21 drill cores were prepared to determine their mineralogy and the chemical characteristics of the minerals.

The mineralogical characteristics of the ore minerals were documented using reflected and transmitted light microscopy, scanning electron microscopy (SEM) and electron-probe micro-analysis (EPMA). SEM was used to evaluate chemical zonation in gold and pyrite grains, mainly due to the presence of Ag and As, respectively. The electron microprobe was used to obtain high-contrast back-scattered images and also for wavelength-dispersion analyses (200 nA beam current, 0.2 seconds per spot) to evaluate the presence of elements undetectable by SEM.

A total of 258 analyses of pyrite and 120 of gold were made with a CAMECA SX50 electron microprobe (Centro de Instrumentación Científica, Universidad de Granada). Natural and artificial standards were used for quantitative analyses. The operating conditions were: accelerating potential 30 kV, beam current 30 nA, and between 60 and 300 seconds of acquisition time on X-ray peaks and background. Selected analyses were also done for Au in pyrite crystals, with a beam current of 100 nA and acquisition times of 2000 seconds on X-ray peak and background. The detection limit reached under these conditions is 475 ppm, 95% confidence.

MINERALOGICAL FEATURES

In the Palai–Islica area, mineralization generally seems associated with veins and veinlets of quartz enclosed within the altered volcanic rocks, and, to a much lesser extent, as disseminations or associated with massive silicification in the uppermost area of the deposit. The Palai–Islica mineralization is of the Fe–Cu–Au type and consists principally of iron sulfides (pyrite, pyrrhotite and marcasite). Chalcopyrite, sphalerite and galena can also be significant, and gold, tetrahedrite–tennantite, bismuthinite, Ag±Bi±Pb±Cu sulfosalts, tellurides, Ag sulfides, bornite, chalcocite, covellite, stannite, and niccolite are minor phases. Oxides of Fe, Ti and Sn are also very common (Carrillo *et al.* 1999, Morales *et al.* 2000).

Iron sulfides (pyrite, marcasite and pyrrhotite) are the major ore minerals in this deposit, with pyrite as the predominant phase, with a wide variety of textures and chemical compositions. Given the close relationship between gold and pyrite in this deposit, characterization of the latter should be useful in understanding gold genesis. We have therefore undertaken a detailed study of these minerals. In Tables 1a, 1b and 2, we summarize the types of pyrite identified (Figs. 2, 3). On the basis of their textural features and chemical variety, the existence of seven types of pyrite is noteworthy (Carrillo *et al*. 2001b). In such types of pyrite, some minor elements were detected, As (up to 3.36% at.), Co (up to

TABLE 1a. ATTRIBUTES OF MEDIUM- TO COARSE-GRAINED PYRITE, IN THE PALAI–ISLICA DEPOSIT, SOUTHEASTERN SPAIN

Type	Textural features	Minor elements	Distribution	Figure
Type I	Massive	As	Enriched zones (cores or internal zones of crystal)	2A (1)
			Polygonal bands	2A (2)
			Irregular concentric bands	2B
Type II	Massive	Co–Ni	Core or internal zones of crystals	2C
			Irregular concentric bands	2C
Type III	Massive	Pb–Bi	Bands along crystallographic directions, with inclusions of galena	2D
Type IV	Porous (core) or massive (rim)	Pure		2A, 2B. 2C, 2D

Note: Types I, II and III are always hosted by pyrite of type IV. Here, medium- to coarse-grained pyrite implies a grain diameter greater than 20 μm In all cases, the mode of occurrence of the pyrite is either disseminated in volcanic rocks, disseminated, granular or massive aggregates in veins with quartz, or associated with massive silicification. In terms of habit, the pyrite may be idiomorphic (cubes, pyritohedra), subidiomorphic or xenomorphic.

0.49% at.) and Ni (up to 0.70% at.) being the most abundant. In all types of pyrite, Au was invariably below the detection limit of EPMA, even in the low-detection-limit analysis performed for Au in As-rich pyrite (Fig. 4).

TABLE 1b. ATTRIBUTES OF FINE-GRAINED PYRITE, IN THE PALAI–ISLICA DEPOSIT, SOUTHEASTERN SPAIN

Type	Occurrence	Textural features	Habit	Minor elements	Figure
Type V	Disseminated, granular or massive aggregates in veins with quartz	Framboidal	Pseudo-framboids	As (low values)	3A
"	"	"	Framboids *sensu stricto*	"	3B
Type VI	"	Colloform banding, Porous	Colloform banding, massive	As (Ag, Cu)	3C
"	" or with massive silicification	Colloform banding, massive		As, Sb (Ag, Cu), compositional banding	3D
Type VII	Disseminated, granular or massive aggregates in veins with quartz	Microgeodes	Xenomorphic	Poor in minor elements	3E
		Banded pyrite in chalcopyrite	Xenomorphic	Poor in minor elements	3F

Here, fine-grained pyrite implies a grain diameter less than 20 μm.

The mineralogy and textures of gold

In this study, we examined 178 gold grains from the different subhorizontal gold-bearing horizons. The longest axis of the grains varied from 2 to 350 μm, and their morphology is highly variable: irregular, subrounded, oval, colloform and subidiomorphic. In the last case, the crystal faces appear in detail as warped surfaces rather than rectilinear planes. On the basis of microscopic examination and the textural relations between the gold grains and other minerals, we were able to distinguish three types of gold (Table 3), of which types A and B both appear mainly in the deepest mineralized horizons (within the area of the LGA and UGA geochemical anomalies), whereas type-C gold was found only in the mineralized horizon closest to the surface.

Grains of *type-A gold* appear in quartz veins with sulfides, included in medium- to coarse-grained pyrite having a cubic or pyritohedral habit. This type of gold grain has a subrounded or subidiomorphic morphology and is found as gold within pyrite crystals (A1; Fig. 5A), generally in the external parts, but later than the arsenic-rich zones, or as gold located at intergranular positions, between the pyrite crystals making up the aggregates (A2; Fig. 5B).

Grains of *type-B gold* appear in quartz veins with sulfides, overgrowing pyrite crystals. They may in turn be overgrown by other sulfides (galena, chalcopyrite and sphalerite) or even in some cases be later than these sulfides (Figs. 5C, D). These grains of gold normally grow on the flat surfaces of the pyrite faces (Figs. 5D, E), or on irregular surfaces (Figs. 5C, F).

TABLE 2. REPRESENTATIVE COMPOSITIONS OF THE VARIOUS TYPES OF PYRITE, PALAI–ISLICA DEPOSIT, SOUTHEASTERN SPAIN

Type	S	Fe	As	Co	Ni	Sb	Cu	Zn	Ag	Au	Pb	Bi	Total
I-A wt%	52.05	46.10	0.51	0.06	0.00	0.00	0.00	0.00	0.02	0.16			98.89
I-B	51.31	45.90	2.46	0.06	0.00	0.01	0.02	0.01	0.01	0.03			99.81
I-C	51.89	46.18	2.01	0.06	0.01	0.01	0.02	0.01	0.01	0.01			100.21
II	52.86	46.04	0.04	0.54	0.00	0.02	0.00	0.02	0.00	0.02			99.53
II	53.15	45.94	0.00	0.05	0.33	0.02	0.00	0.01	0.00	0.03			99.53
III	52.79	45.90	0.31	0.06	0.00	0.00	0.01	0.00	0.04	0.04	0.50	0.37	99.14
IV	53.46	46.68	0.00	0.08	0.01	0.01	0.01	0.01	0.01	0.01			100.27
V-A	53.08	45.96	0.21	0.08	0.01	0.02	0.02	0.00	0.02	0.04			99.43
V-B	52.80	45.19	0.12	0.09	0.05	0.01	0.00	0.01	0.06	0.00			98.33
VI-A	51.51	43.82	3.28	0.06	0.07	0.21	0.35	0.09	0.11	0.03			99.52
VI-B	50.47	43.34	5.45	0.05	0.00	0.37	0.16	0.01	0.17	0.00			100.01
VII-A	52.57	46.40	0.01	0.085	0.00	0.013	0.01	0.00	0.00	0.03			99.02
VII-B	51.75	46.26	0.00	0.06	0.00	0.01	0.00	0.00	0.02	0.00			98.11
I-A at.%	66.05	33.59	0.28	0.04	0.00	0.00	0.00	0.00	0.01	0.03			100.00
I-B	65.13	33.45	1.34	0.04	0.00	0.00	0.02	0.01	0.00	0.01			100.00
I-C	65.42	33.43	1.08	0.04	0.01	0.01	0.01	0.00	0.00	0.00			100.00
II	66.39	33.20	0.02	0.37	0.00	0.01	0.00	0.01	0.00	0.00			100.00
II	66.65	33.08	0.00	0.04	0.22	0.01	0.00	0.00	0.00	0.01			100.00
III	66.44	33.16	0.17	0.04	0.00	0.00	0.00	0.00	0.01	0.01	0.10	0.07	100.00
IV	66.56	33.36	0.00	0.05	0.01	0.01	0.00	0.01	0.00	0.00			100.00
V-A	66.66	33.14	0.11	0.05	0.01	0.01	0.01	0.00	0.01	0.01			100.00
V-B	66.92	32.89	0.06	0.06	0.03	0.00	0.00	0.01	0.02	0.00			100.00
VI-A	65.66	32.06	1.79	0.04	0.05	0.07	0.22	0.05	0.04	0.01			100.00
VI-B	64.75	31.92	2.99	0.04	0.00	0.13	0.10	0.00	0.06	0.00			100.00
VII-A	66.31	33.61	0.01	0.06	0.00	0.00	0.01	0.00	0.00	0.01			100.00
VII-B	66.05	33.89	0.00	0.04	0.00	0.00	0.00	0.00	0.01	0.00			100.00
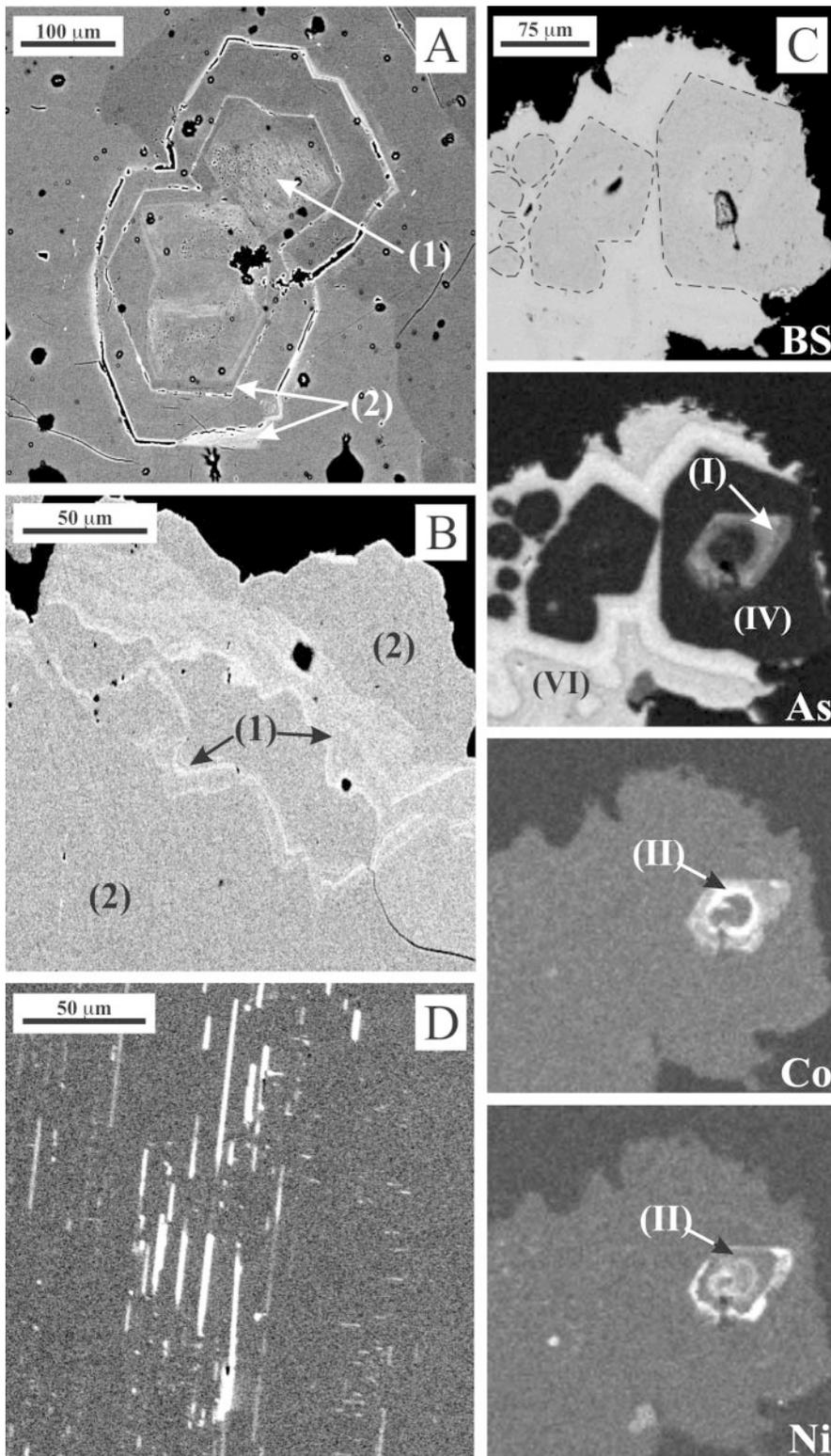
Grains of *type-C gold* appear in areas of massive silicification. Unlike the previous types, type-C grains (Fig. 5G) do not occur in association with pyrite, but are found as "free" grains in the gangue, around the edges of spaces left by dissolution of phenocrysts in volcanic rock. Type-C grains are the smallest in size, and the only ones that may have a colloform morphology.

Of all the varieties of pyrite identified (Tables 1a, 1b), the gold of types A and B was found exclusively with medium- to coarse-grained pyrite (of higher purity). These gold grains began to crystallize at an advanced stage of pyrite precipitation, and their formation was completed when most of the pyrite had already crystallized, as can be deduced from textural relations between gold and the different types of pyrite.

CHEMICAL COMPOSITION OF GOLD

According to results of SEM and EPMA data (Table 3), the three types of gold distinguished by their textural characteristics also present different chemical characteristics, depending on the Ag content, whereas the content of other elements is low (Table 4).

Type-A gold

The composition of this type corresponds to that of Au–Ag alloys in which the Ag content varies from 2.34 to 33.96 at.%. Grains of this type are rather homogeneous, with few compositional variations observed within each grain, as inferred from the back-scattered images of the grains analyzed. Only one grain of type-A gold shows a core slightly enriched in Ag (up to 2.50%) with respect to the rim (Fig. 6).

In addition to the textural differences found in subtypes A1 and A2, we also observed slight compositional differences between them. Subtype A1 has the lowest Ag values of all the Au–Ag alloy compositions, with an Au/(Au + Ag) value of 0.693 to 0.975 (average value 0.869); most values are from 0.784 to 0.975 (Fig. 7). In contrast, gold grains of subtype A2 are slightly richer in Ag, with the broadest range of Au/(Au + Ag) values observed (0.633–0.968, average 0.851; Fig. 7). In samples in which both types A1 and A2 of gold grains

were found, we also observed a trend toward higher Ag content in the A2 type of gold grains.

Among A1-type gold grains, we detected small differences between the gold grains according to the morphology of the pyrite in which they were contained. Gold included in pyrite with a pyritohedral habit had a slightly lower Ag content [mean Au/(Au + Ag): 0.887] than those contained in pyrite with a cubic habit [mean Au/(Au + Ag): 0.856].

The overall concentration of the minor elements was invariably less than 6.5 at.%. The most abundant were Fe (0.13–5.37%) and S (0.17–6.39%), the latter due to contamination by the host pyrite. However, Fe is ambiguous since the Fe:S ratio (Fig. 8) is commonly lower than that dictated by pyrite stoichiometry. Finally Bi (0.01–0.17%), Cu (0–0.32%), Hg (0–0.12%), Te (0.02–0.16%) were invariably present at very low concentrations (Table 4).

Type-B gold

The chemical characteristics of this type also correspond to Au–Ag alloy, with a higher Ag content (13.30 to 41.92%) than the type-A alloy. Unlike the type-A grains, those of type B commonly present marked chemical zonation, with up to 18.89% variation of Ag content in a single grain (Fig. 6). This chemical zona-

TABLE 3. TYPES OF GOLD GRAINS IN THE PALAI–ISLICA DEPOSIT, SOUTHEASTERN SPAIN

Type, subtype		Occurrence	In relation with		Habit	Ag content, distribution	Fig.
A	A1	In veins of quartz with sulfides	Crystals of type-IV pyrite	Inside crystals of type-IV pyrite, near the rim	sub-rounded, sub-idiomorphic	2.34 – 28.91% homo-geneous	4A
	A2	"	"	Intergranular positions in pyrite aggregates	"	3.04 – 33.96%, homo-geneous	4B
B	B1	"	"	On pyrite faces or irregular surfaces of pyrite	Xeno-morphic	13.90 – 38.99%, mosaic grains	4E
	B2	"	" with Gn, Ccp and Sp	Overgrowth on crystals of pyrite, over-grown by other BM sulfides or intergranular*	Xeno-morphic	22.44 – 33.30%, mosaic grains	4C, 4D, 4F
C		In zones of massive silicification	"Free" in the gangue	In cavities due to the dissolution of phenocrysts in volcanic rocks	Colloform	0 – 0.25%, homo-geneous	4G

Symbols: BM: base-metal, Gn: galena, Ccp: chalcopyrite, Sp: sphalerite.
* Intergranular between the two minerals. The Ag contents are expressed in % (atom).

FIG. 2. Back-scattered SEM images (BS) of medium- to coarse-grained pyrite (>20 μm). (A) Type-I pyrite rich in As overgrown by type-IV pyrite: (1) core of porous pyrite, (2) polygonal bands. (B) Irregular concentric bands of As-rich type-I pyrite (1), alternating with type-IV pyrite (2). (C) Back-scattered SEM image of different pyrite types (I, II and IV) (inside dotted lines) overgrown by type-VI colloform pyrite (outside dotted lines) and their X-ray images for As, Co and Ni. (D) Bands of type-III (Pb–Bi-bearing) pyrite, following crystallographic directions.
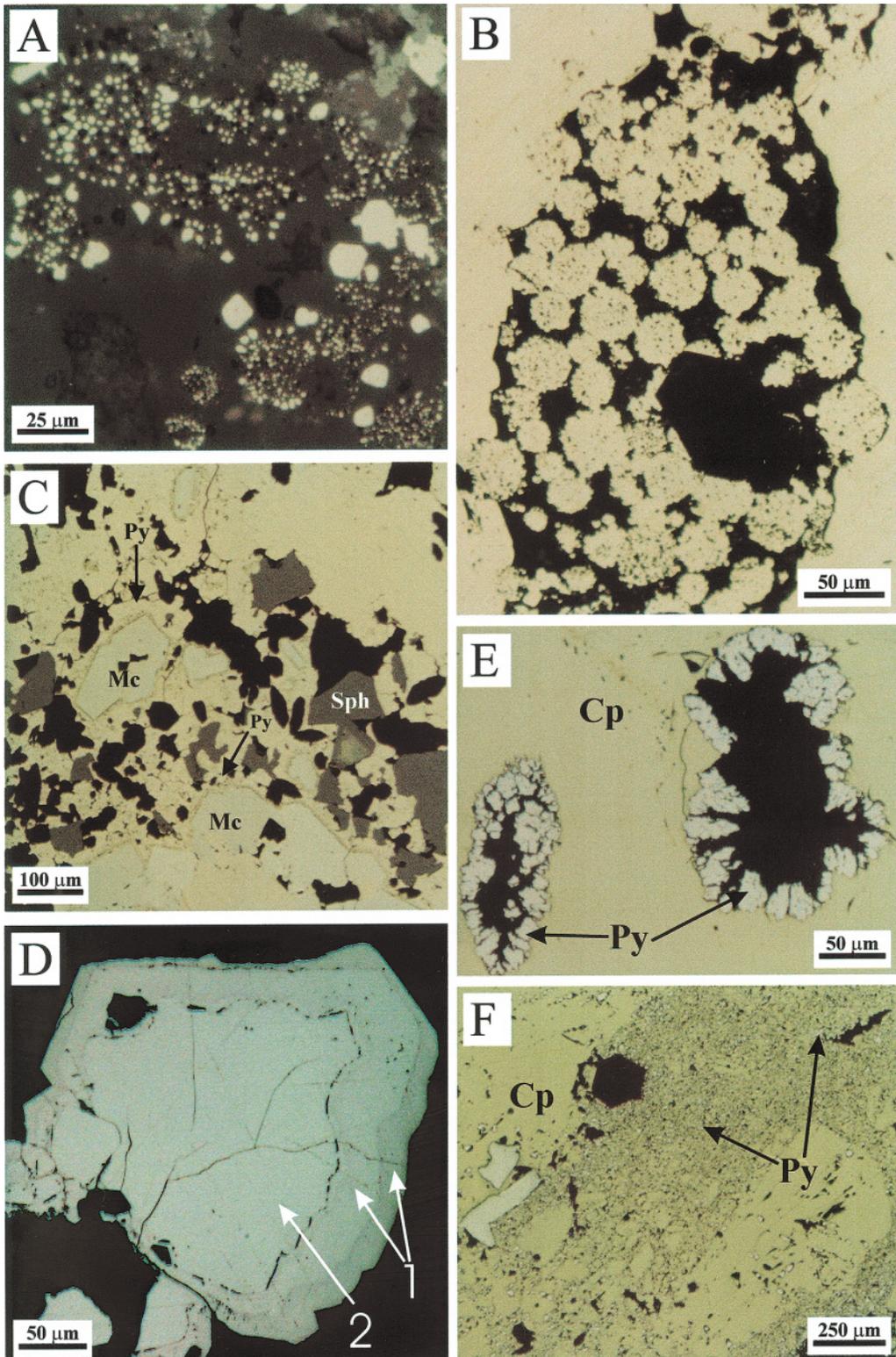
tion is sharp, and, as seen in the back-scattered image, has well-differentiated domains (Fig. 9A), one light-colored (Ag-poor) and the other dark (Ag-enriched). The Ag-poor zones generally rim the grains (Figs. 9A, B), but in some cases they make up a mesh-like pattern (Fig. 9C) bounding the Au-rich zones. The evolution observed in grains of type-B gold, unlike that shown by type-A gold grains, is toward higher Ag contents as growth continues.

Moreover, some differences can be detected in grains of type B (Fig. 7) between those not overgrown by base-

TABLE 4. THE COMPOSITION OF GOLD GRAINS FROM PALAI-ISLICA DEPOSIT, SOUTHEASTERN SPAIN

	Type A1 (n = 30)				Type A2 (n = 23)				Type B1 (n = 46)				Type B2 (n = 11)				Type C (n = 10)			
	Min	Max	Ave	SD	Min	Max	Ave	SD	Min	Max	Ave	SD	Min	Max	Ave	SD	Min	Max	Ave	SD
Au	79.96	98.13	91.67	4.87	75.34	97.50	90.93	5.87	70.95	97.21	84.81	3.68	72.53	85.35	82.18	7.00	91.84	100.81	97.12	3.17
Ag	1.38	19.49	7.69	4.34	1.71	23.94	8.97	5.74	3.48	28.53	14.50	4.36	13.75	26.07	18.60	6.94	0.00	1.82	0.68	0.80
S	0.06	0.37	0.14	0.07	0.07	1.30	0.21	0.26	0.05	0.93	0.11	0.12	0.03	0.49	0.13	0.13	0.01	0.45	0.18	0.16
Bi	0.00	0.19	0.09	0.05	0.03	0.19	0.08	0.04	0.00	0.26	0.08	0.04	0.05	0.19	0.11	0.05	0.02	0.22	0.12	0.07
Fe	0.03	1.75	0.76	0.52	0.04	2.10	0.76	0.71	0.00	1.48	0.32	0.47	0.06	1.77	0.31	0.43	0.00	0.78	0.20	0.27
Te	0.01	0.11	0.09	0.02	0.06	0.13	0.10	0.02	0.08	0.14	0.10	0.01	0.09	0.13	0.11	0.02	0.05	0.10	0.08	0.02
Cu	0.00	0.11	0.02	0.03	0.00	0.00	0.00	0.02	0.00	0.44	0.03	0.74	0.00	2.56	0.23	0.09	0.00	0.23	0.04	0.07
Hg	0.00	0.14	0.04	0.04	0.00	0.12	0.03	0.04	0.00	0.23	0.07	0.04	0.03	0.16	0.09	0.06	0.01	0.12	0.05	0.04
Se	0.00	0.02	0.01	0.01	0.00	0.02	0.00	0.00	0.00	0.02	0.00	0.00	0.00	0.00	0.00	0.00	0.00	0.02	0.01	0.00
Fn	805	986	922	44	759	982	910	58	714	965	854	41	736	860	816	70	982	1000	993	8
Au	65.23	94.17	83.92	7.07	58.52	95.44	82.13	10.00	57.24	93.16	75.31	5.67	59.88	75.73	69.25	10.30	93.32	99.33	96.63	1.81
Ag	2.34	28.91	12.59	6.52	3.04	33.96	14.19	8.18	6.12	41.92	22.78	5.78	22.44	39.30	28.36	9.71	0.00	3.19	1.19	1.40
S	0.37	2.00	0.77	0.37	0.38	6.39	1.11	1.27	0.27	4.52	0.59	0.57	0.17	2.34	0.64	0.62	0.07	2.78	1.09	1.01
Bi	0.00	0.17	0.08	0.05	0.02	0.17	0.07	0.04	0.00	0.22	0.07	0.03	0.04	0.14	0.09	0.04	0.02	0.21	0.11	0.07
Fe	0.11	5.37	2.41	1.59	0.12	5.90	2.28	2.05	0.00	4.16	0.95	1.26	0.17	4.83	0.88	1.26	0.00	2.84	0.69	0.96
Te	0.02	0.16	0.13	0.03	0.09	0.17	0.13	0.02	0.11	0.18	0.14	0.02	0.11	0.18	0.14	0.02	0.08	0.15	0.12	0.02
Cu	0.00	0.32	0.06	0.07	0.00	0.00	0.00	0.05	0.00	1.18	0.09	1.77	0.00	6.16	0.56	0.23	0.00	0.66	0.11	0.20
Hg	0.00	0.12	0.04	0.04	0.00	0.10	0.03	0.03	0.00	0.19	0.06	0.03	0.03	0.13	0.07	0.05	0.01	0.12	0.05	0.04
Se	0.00	0.05	0.01	0.01	0.00	0.04	0.01	0.01	0.00	0.06	0.01	0.00	0.01	0.01	0.01	0.01	0.01	0.04	0.02	0.01
Au*	0.693	0.975	0.869	0.069	0.633	0.968	0.851	0.088	0.577	0.938	0.767	0.056	0.604	0.771	0.710	0.100	0.968	1.000	0.988	0.30

n: number of analyses done. Min: minimum, Max: maximum. Ave: average. Fn: fineness, defined as [Au/(Au + Ag)] × 1000, where concentrations are expressed in wt%. Au* = Au/(Au + Ag), where concentrations are expressed in at.%. The composition of gold grains is first expressed in wt%, then in at.%. SD: standard deviation (1σ).

FIG. 3. Reflected-light photomicrograph of fine-grained pyrite (<20 μm). (A) Pseudoframboidal type-V pyrite in quartz. (B) Type-V framboidal pyrite in a cavity in type-IV pyrite. (C) Type-VI porous colloform pyrite overgrowing marcasite and sphalerite crystals. (D) Bands of massive, brown, colloform type-VI pyrite (1), overgrowing type-IV coarse-grained pyrite (2). (E) Microgeodes of xenomorphic crystals of type-VII pyrite in chalcopyrite. (F) Banding in xenomorphic crystals of type-VII pyrite with chalcopyrite.
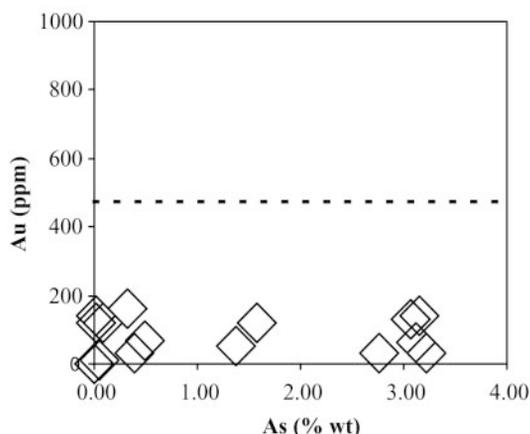

FIG. 4. As *versus* Au content in pyrite using high-acquisition-time analyses in order to obtain lower detection limit. Dashed line: detection limit of gold.
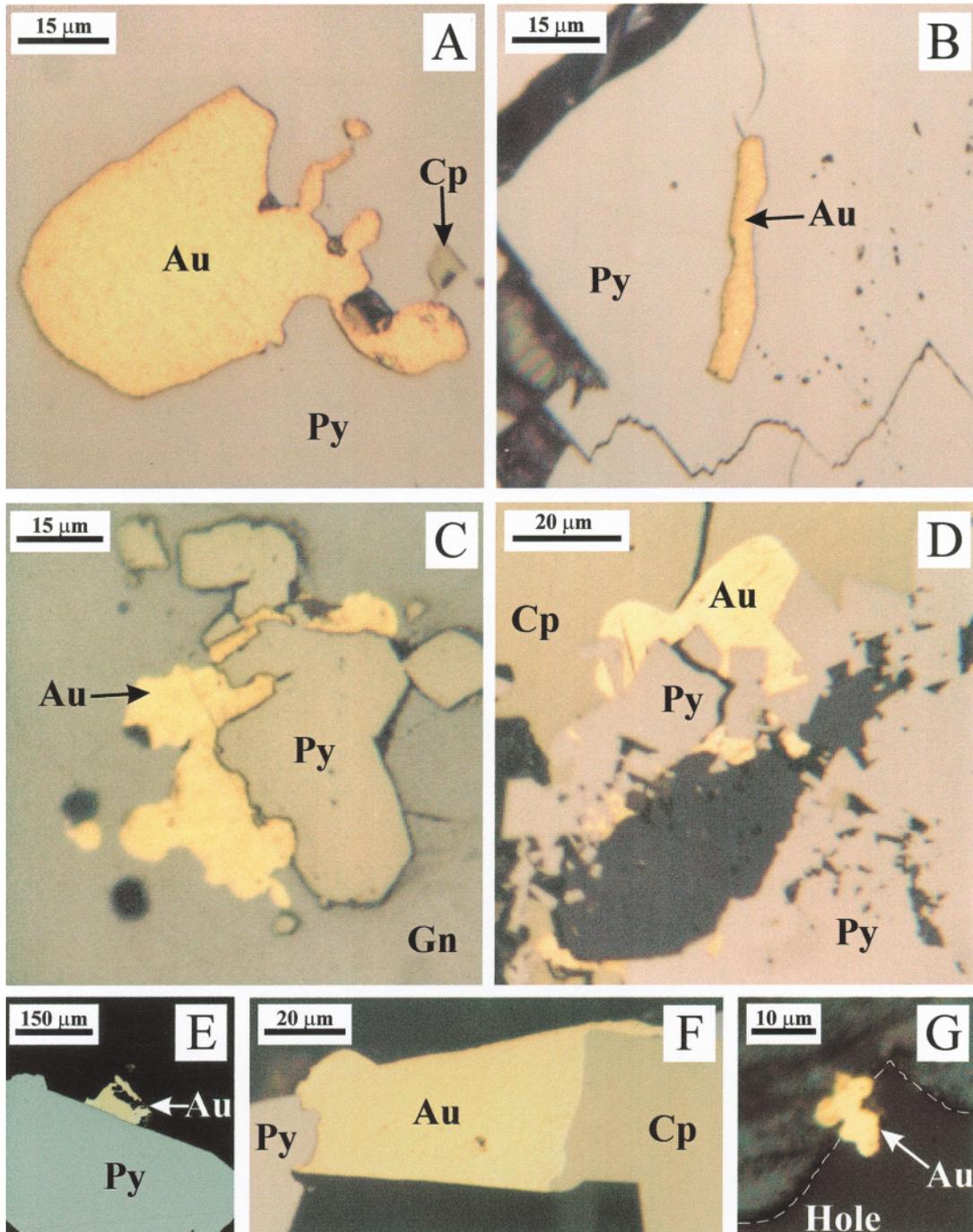
FIG. 5.   Reflected-light photomicrograph of gold grains. (A) Subrounded grain of subtype-A1 gold included in type-IV pyrite. (B) Intergranular subtype-A2 grain in a pyrite aggregate. (C, D) Type-B gold grains overgrowing pyrite and, in turn, overgrown by galena (C) and chalcopyrite (D). (E, F) Type-B gold grains overgrowing pyrite on planar (E) or irregular (F) surfaces. (G) Type-C gold grain in a cavity in altered volcanic rock.
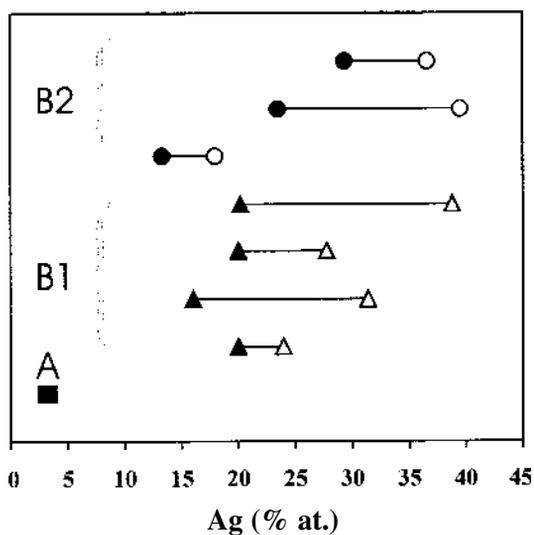
FIG. 6. Ag content of different zoned grains of gold. In order to see the magnitude of the zonation in a single grain, we have placed the results of analysis of a single grain above each line (■: type A, ▲: subtype B1, ●: subtype B2; black: core, white: rim).
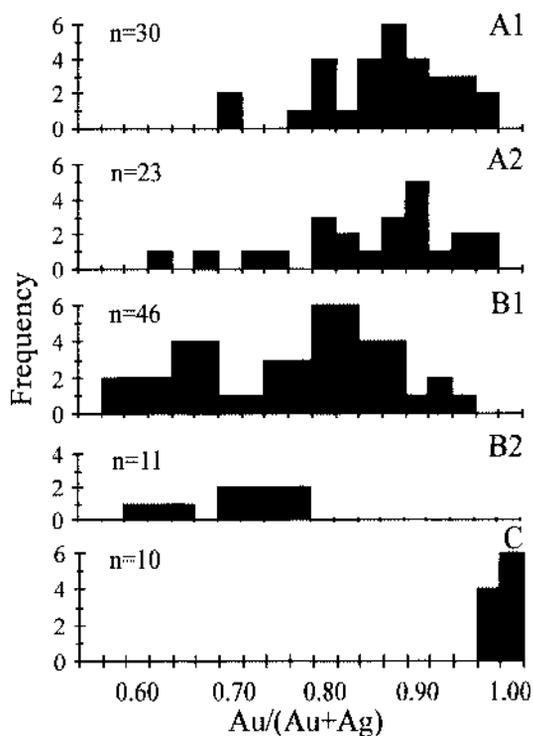
FIG. 7. Frequency histograms for the Au/(Au + Ag) value in the different types (A1, A2, B1, B2 and C) of gold grains analyzed.
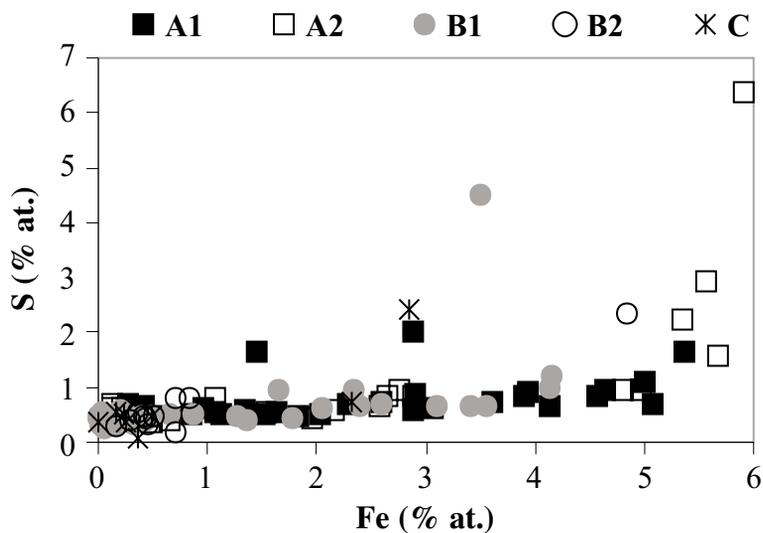
FIG. 8. Content of Fe *versus* that of S in gold grains.

metal sulfides (subtype B1) and others that are so overgrown (subtype B2). The latter have a narrower compositional range and a higher Ag content [Au/(Au + Ag) from 0.604 to 0.771, average 0.710] than the former [Au/(Au + Ag) from 0.577 to 0.938, average 0.767].

The minor elements in type-B gold fall in a very similar range with respect to type-A gold. However, there are some differences: a drop in the Fe (0–4.83%) and S (0.17–4.52%) content could be related to lower contamination by the pyrite. A more subtle difference is a slightly higher concentration of Hg (average 0.6% in grains of type B with respect to an average value of 0.03% in grains of type A].

Type-C gold

This type corresponds to native gold with limited Au/(Au + Ag) values, from 0.968 to 1.000 [average Au/(Au + Ag) value = 0.988; Fig. 7]. There are no important differences in minor-element contents with the other two types of gold, apart from a lower concentration of S (0.07–2.78%), Fe (0–2.84%) and Bi (on average, 0.11 at.%).

DISCUSSION

Chemical composition of the gold grains

Gold and silver are the major elements of the alloys, and the paucity of other elements is noteworthy. Taking into consideration the fineness values [Au/(Au + Ag) × 1000, concentrations in wt.%] compiled by Morrison

et al. (1991) for different types of epithermal deposits, the values measured in the Palai–Islica deposit, in the range from 714 to 986, agree very well with those proposed by these authors for andesitic environments (720–980), such as at Palai–Islica. These values are intermediate between those proposed for other environments: 0–880 in "adularia–sericite"-type environments, 900–1000 in "acid-sulfate" environments, and 520–969 in "Au–Te–Se" environments.

With regard to the minor-element contents of the Au–Ag alloy in Palai–Islica, only Fe reaches significant concentrations. These Fe values may be due to any of three factors: (1) contamination from the host pyrite, (2) secondary fluorescence of the Fe$K\alpha$ line of the host pyrite caused by Au$L\alpha$ radiation during analysis (Healey & Petruk 1990), or (3) presence of Fe in the alloy, as proposed by Boyle (1979), Krupp & Weiser (1992) and Kucha *et al.* (1994). Although some of the Fe may be due to direct contamination from the host pyrite, not all of it can be justified in this way, since on the one hand, the Fe:S ratio (Fig. 8) is very high (higher than stoichiometric values for pyrite) and on the other, the values are systematically high, even for large-size grains, for which contamination should be more difficult. In cases free of contamination, we cannot therefore be sure whether the Fe values result from secondary fluorescence of the Fe$K\alpha$ of the host pyrite produced by the Au$L\alpha$ radiation of the alloy grains. The fact that the mean Fe values in type-A grains are generally much higher than the mean values obtained for type-B grains suggests that part of the Fe content is due to pyrite fluorescence. Nonetheless, we cannot discount the possibility that part
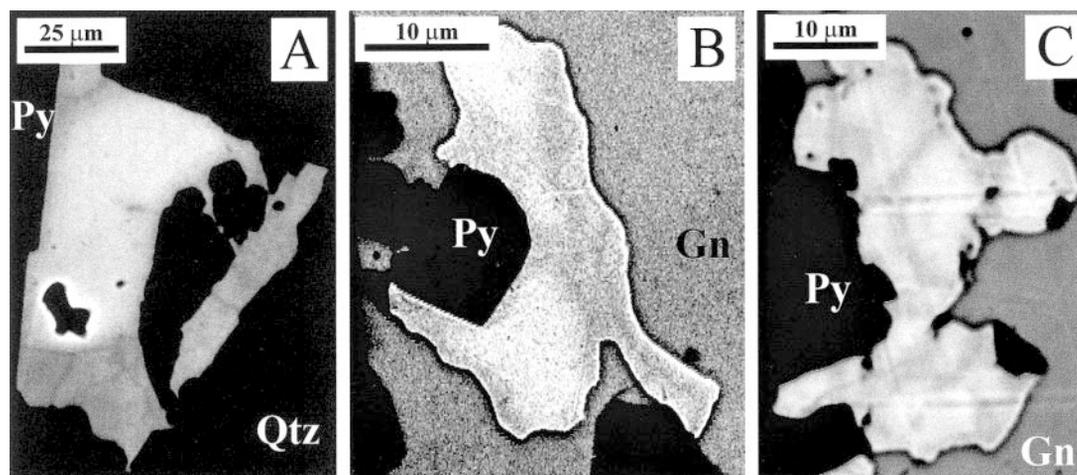

FIG. 9.   Back-scattered SEM images of zoned type-B gold grains. (A, B) Two clearly differentiated domains, one light-colored (Au-rich) and the other dark (Ag-rich), with the lighter-colored domains internal with regards to the darker ones. (C) Dark areas bound light-colored areas.

of the Fe reported really corresponds to Fe contained in the alloy grains.

Gold content of pyrite

All the Au values obtained by EPMA in the different types of pyrite are similar (mean 0.02 wt%) and well below the detection limit for Au in pyrite (0.32 wt%, or 0.05% in the case of high-acquisition-time analyses), but they are useful as an indicator that the content of "invisible" gold is low compared to the values of 100 to 1300 ppm found in the literature (Cook & Chryssoulis 1990, Arehart *et al.* 1993, Fleet & Mumin 1997, Cabri *et al.* 1998, Asadi *et al.* 1999, Kojonen & Johanson 1999, Ashley *et al.* 2000). Moreover, in the Palai–Islica pyrite, there is no correlation between As and Au (Fig. 4), which is a characteristic commonly mentioned for pyrite with "invisible" gold by the aforementioned authors. Together with the relative abundance of free gold, this indicates that the proportion of "invisible" gold in the "total" gold of the deposit is practically nil.

Evolution of gold grains and their relation to iron sulfides

We can infer a sequence in the precipitation of the Au–Ag alloy on the basis of textural and chemical characteristics. This sequence begins with the formation of type-A gold grains, which are included in pyrite after formation of the arsenic zonation and before the end of pyrite precipitation. These first Au–Ag grains are richest in Au, this concentration decreasing in the alloys as precipitation advances. Given the simultaneous growth of gold and precipitation of pyrite, the latter encapsulated and sealed the gold, so that the gold grains formed in this first stage are homogeneous. When pyrite precipitation ceased, precipitation of type-B gold and the base-metal-bearing sulfides took place, so that the type-B gold is included in the galena, sphalerite or chalcopyrite. In some cases, the gold could even postdate the formation of the base-metal sulfides. We assume that there is a hiatus between pyrite and base-metal-bearing sulfides. Thus, encapsulation of gold grains is not immediate, leading to their "open" character, explaining the common appearance of zoned grains (rim enriched in Ag in comparison with the core), thus marking a general evolution of the Au–Ag alloy by an increase in Ag content as precipitation continued. This evolution, given the bimodal character of the zoned grains, does not seem to have been continuous.

Type-C gold, given the host-rock characteristics, as well as the gold textures and chemical characteristics, appears to have a different genesis than types A and B. Its origin could be due to magmatic fluids depositing native gold and causing associated silicification in the uppermost levels of the deposit. Both the textures (fine grained) and the composition of gold (almost free of Ag) suggest a secondary origin (*i.e.*, Benedetti & Boulègue 1991, Krupp & Weiser 1992, Hong 2000), but this hypothesis is rejected for the following reasons. a) The mineralogy of the massive silicification, leading to a volcanic rock replaced completely by quartz with pyrite precipitation, is inconsistent with an oxidative low-temperature environment. The sulfide assemblage lacks any trace of the oxidation process, such as sulfate replacement of sulfides. In addition, there is no evidence of supergene enrichment in sulfide. b) The occurrence of massive silicification surrounded by argillic alteration (Morales *et al.* 2000) is indicative of a hypogene origin. c) Stable isotope data ($\delta^{18}O_{Qtz}$ between 12.2 and 17.8‰: Carrillo *et al.* 2001c) and fluid-inclusion data (Carrillo *et al.* 2002) also suggest a hydrothermal magma-related genesis for this massive silicification.

Causes of the variation of Au:Ag in the alloy

According to Gammons & Williams-Jones (1995), the changes in the composition of the Au–Ag alloy (types A and B) could be the result of several factors: temperature, $f(S_2)$, $f(O_2)$, concentration of Cl⁻, pH and Au:Ag ratio in the system. In the case of Palai–Islica, it is not easy to discover which of these factors affected the compositional evolution of the Au–Ag alloy. However, the data available at present allow us to state the following: (1) There was a *temperature decrease*, which is consistent with the data on fluid inclusions (between 125–450°C) obtained by Morales *et al.* (2000). This decrease is consistent with a higher Ag content of Au–Ag alloy (Shikazono & Shimizu 1987) and could explain the chemical evolution of the Palai–Islica gold grains. (2) There was a *decrease of $f(S_2)$*, inferred from the variation in the composition of sphalerite determined in the Palai–Islica deposit (Fe in sphalerite ranges from 0.08 to 9.72 at.%; authors' data, in prep.). This drop in $f(S_2)$ resulted in a higher Ag content of the Au–Ag alloy (Gammons & Williams-Jones 1995), in all cases with a Au:Ag ratio less than 1, which is a condition fulfilled at Palai–Islica (Morales *et al.* 2000). (3) There was a *decrease of the Au:Ag ratio in the mineralizing fluid*, which was caused by a decrease of Au in the residual fluid, or by entry of Ag into the system, as precipitation of the Au–Ag alloy continued. This decrease could also lead to the formation of alloy richer in Ag and the formation of other Ag-bearing mineral phases like tetrahedrite–tennantite, Ag ± Bi ± Pb ± (Cu) sulfosalts, and Ag-bearing sulfides at the latest stages of the paragenetic sequence (Carrillo *et al.* 2001a). (4) In the specific case of type-B zoned grains, apart from the three factors mentioned above, variation in the Ag content could also have been caused by the adsorption–reduction process that caused this type of gold grain. This process would be consistent with the experimental observations of Scaini *et al.* (1996), who obtained gold grains growing on the surface of pyrite, with a higher content of Ag toward the rim of the gold grain.

Transport and precipitation mechanisms of Au and Ag

According to Seward & Barnes (1997), gold transport mainly occurs through sulfide complexes in epithermal systems with conditions of the mineralizing fluid such as described by Morales *et al.* (2000) for the mineralized veins in the Palai–Islica deposit (T < 350°C, low to moderate salinity, and moderate to low pH). However, the characteristics of the fluids in the uppermost areas of the deposit are significantly different [high $f(O_2)$ and low pH]. Such conditions would have led to the crystallization of very pure gold (Krupp & Weiser 1992) on the basis of the destabilization of thiosulfate-type complexes (Kucha *et al.* 1994).

As for the transport mechanism of Ag, there is less certainty about the nature of the transporting complex (Seward & Barnes 1997, Gammons & Barnes 1989); given the characteristics of the Palai–Islica mineralization, we infer that the complexes were mainly of the $Ag(SH)_2^-$ type.

The characteristics of the three types of gold described in this paper could correspond to different mechanisms of precipitation. For type-A gold, the principal mechanism of precipitation could be oversaturation of gold in the fluid caused by variations in the physical and chemical factors, mainly by a decrease in the activity of sulfide complexes in the fluid (Benning & Seward 1996). The initial precipitation of gold probably coincides with a decrease in sulfur activity caused by precipitation of a significant volume of pyrite. Furthermore, as this was the "first" gold to precipitate, the concentration of Au in the fluid likely would have been higher than at later stages, at which point it would have been easier to reach oversaturation. Apart from these two factors, there is no indication of the requirements necessary for the accumulation of gold by any other mechanism, such as by a surface process. For example, we did not observe any chemical defects in the host pyrite (it is very pure) that could have given it special conductive properties (Moller & Kersten 1994) favoring electrochemical precipitation, nor did we observe interruptions in the deposit that would have allowed an important accumulation of gold by adsorption and reduction. The interface between arsenian pyrite and pyrite without trace elements, which could be a preferred place for the accumulation of gold by electrochemical processes owing to the presence of an n–p junction, which causes the reduction of Au^+ and the precipitation of gold (Moller & Kersten 1994), never contains visible gold. Moreover, a sorption mechanism (*i.e.*, Renders & Seward 1989) would lead to formation of invisible gold, and also to formation of visible gold if the precipitation of pyrite were sufficiently slow. However, we did not detect invisible gold in any of the types of pyrite.

Another mechanism of gold precipitation may be the decrease of temperature. However, this is a less important factor since the drop in temperature documented with T_h values (Morales *et al.* 2000) affected the overall deposit and was not restricted to the gold-rich zones. However, fluids associated with gold horizons suggest boiling or mixing processes (Morales *et al.* 2000), which again point to a decrease in the concentration of reduced sulfur.

In the case of *type-B gold*, the principal mechanism of precipitation could have been adsorption–reduction, so that Au precipitation could have been conditioned by electrochemical factors and the chemical and physical conditions of the pyrite surface on which it grew (Renders & Seward 1989, Hyland & Bancroft 1989). According to Kucha *et al.* (1994), the pyrite surface first adsorbs the gold-bearing complexes and then reduces them, precipitating Au (and Ag) as metal. The argument in favor of this hypothesis is the systematic localization of type-B gold on the faces of pyrite crystals. Usually, these grains grow adapting to the pyrite surface, reflecting a surface control by the pyrite during the growth of gold particles, with either planar contact or infilling of cavities in the pyrite. These physical defects of the pyrite surface could have aided the electrical accumulation that induces the reduction of the Au of the hydrothermal fluid (Starling *et al.* 1989). In the case of pyrite–chalcopyrite contacts, a p-type conductivity take place (Moller & Kersten 1994), favoring the accumulation of gold (Fig. 5D). Unlike the type-A grains, the formation of type-B gold did not coincide with an important precipitation of sulfide, such that sulfur activity presumably was constant. In addition, if there was no entry of Au and Ag into the system, the contents of these elements in the mineralizing fluid must have been low after precipitation of the type-A gold, and so it would have been more difficult to reach oversaturation. The electrochemical process leads to the formation of visible gold even with a low content of Au in the fluid (Moller & Kersten 1994).

The main mechanism of precipitation of type-C gold may well involve colloidal suspensions (Saunders 1994). In favor of this mechanism is the existence of gold grains with colloidal growths, the tiny size of these grains in association with colloform pyrite, and the association of gold with masses of quartz, which could originally have been amorphous silica (Saunders 1994).

Conclusions

(1) Of all the different textural varieties of pyrite studied, the unzoned medium- to coarse-grained pyrite is the only one bearing gold.

(2) The main *gold-bearing phases* in the Palai–Islica deposit are Au–Ag alloy and native gold. The content of "invisible" gold in pyrite is practically nil.

(3) A clear distinction can be established between three types of gold, each with a different genesis, on the basis of their textural and chemical characteristics. On the one hand, there is the Au–Ag alloy (types A and B), which is the form in which the gold appears in association with the mineralized veins, and, on the other, there

is native gold (type C), associated with massive silicification in the uppermost areas of the deposit. The type-A alloy originated from variations in the thermodynamic parameters of the system (mainly the decrease in sulfur activity), whereas the formation of the type-B alloy was mainly controlled by electrochemical factors. Type-C gold may have been produced from colloidal solutions at significantly different geochemical conditions.

(4) The chemical evolution of the alloys is characterized by Ag enrichment as precipitation continued. Grains of type-A gold would have been the first to form (encased in the pyrite, with relatively low Ag content and hardly any zonation), followed by the type-B grains (overgrowing the pyrite, with a higher Ag content than the type-A grains and commonly zoned, the "late zones" being richer in Ag). Finally, type-C native gold has practically no Ag.

Acknowledgements

References

AREHART, G.B., CHRYSSOULIS, S.L. & KESLER, S.E. (1993): Gold and arsenic in iron sulfides from sediment-hosted disseminated gold deposits: implications for depositional processes. *Econ. Geol.* **88**, 171-185.

ARRIBAS, A., JR. (1995): Characteristic of high-sulfidation epithermal deposits, and their relation to magmatic fluid. *In* Magmas, Fluids, and Ore Deposits (J.F.H. Thompson, ed.). *Mineral. Assoc. Can., Short Course* **23**, 419-454.

_____, CUNNINGHAM, C.G., RYTUBA, J.J., RYE, R.O., KELLY, W.C., PODWYSOCKI, M.H., McKEE, E.H. & TOSDAL, R.M. (1995): Geology, geochronology, fluid inclusions, and isotope geochemistry of the Rodalquilar gold alunite deposit, Spain. *Econ. Geol.* **90**, 795-822.

_____ & TOSDAL, R.M. (1994): Isotopic composition of Pb in ore deposits of the Betic Cordillera, Spain: origin and relationship to other European deposits. *Econ. Geol.* **89**, 1074-1093.

ASADI, H.H., VONCKEN, J.H.L. & HALE, M. (1999): Invisible gold at Zarshuran, Iran. *Econ. Geol.* **94**, 1367-1374.

ASHLEY, P.M., CREAGH, C.J. & RYAN, C.G. (2000): Invisible gold in ore and mineral concentrates from the Hillgrove gold–antimony deposits, NSW, Australia. *Mineral. Deposita* **35**, 285-301.

BELLON, H., BORDET, P. & MONTENAT, C. (1983): Chronologie du magmatisme Néogène des Cordillères Bétiques (Espagne méridionale). *Bull. Soc. Géol. France* **XXV**, 205-217.

BENEDETTI, M. & BOULÈGUE, J. (1991): Mechanism of gold transfer and deposition in a supergene environment. *Geochim. Cosmochim. Acta* **55**, 1539-1547.

BENNING, L.G. & SEWARD, T.M. (1996): Hydrosulphide complexing of Au(I) in hydrothermal solutions from 150–400°C and 500–1500 bar. *Geochim. Cosmochim. Acta* **60**, 1849-1871.

BOYLE, R.W. (1979): The geochemistry of gold and its deposits. *Geol. Surv. Can., Bull.* **280**.

CABRI, L.J., GASPAR, O.C., LASTRA, R. & McMAHON, G. (1998): Distribution of gold in tin-rich samples from the Corvo orebody, Portugal. *Can. Mineral.* **36**, 1347-1360.

CARRILLO ROSÚA, F.J., MORALES RUANO, S., BOYCE, A.J., FENOLL HACH-ALÍ, P. & FALLICK, A.E. (2001c): Caracterización mediante geoquímica de isótopos estables del depósito epitermal de Palai–Islica (Carboneras, Almería). Datos preliminares. *Bol. Soc. Española Mineralogía* **24–A**, 149-150.

_____, _____, _____, _____ & _____ (2002): El depósito de Au–Cu de Palai–Islica, Carboneras (Almería): ejemplo de la coexistencia de dos tipos de mineralización (de alta y de baja sulfuración) en un ambiente epitermal. *Bol. Soc. Española Mineralogía* **25–A**, 21-22.

_____, _____ & FENOLL HACH-ALÍ, P. (2001a): Mineralogy and mineral chemistry of precious metals of the Cu–Au mineralisation at the Palai–Islica deposit, Almeria, SE Spain. *In* Mineral Deposits at the Begining of the 21st Century (Piestrzyñski A. *et al.*, eds.). Balkema, Lisse, The Netherlands (715-718).

_____, _____ & _____ (2001b): Tipología de la pirita en el depósito epitermal de Palai–Islica (Carboneras, Almeria). Implicaciones en la génesis del oro. *Bol. Soc. Española Mineralogía* **24–A**, 151-152.

_____, _____, _____, DE LA FUENTE CHACÓN, F. & CONTRERAS LÓPEZ, E. (1999): Mineralogía y texturas del depósito aurífero de Palai (Carboneras, Almeria). Datos preliminares. *Bol. Soc. Española Mineralogía* **22–A**, 25-26.

COMAS, M.C., PLATT, J.P., SOTO, J.I. & WATTS, A.B. (1999): The origin and tectonic history of the Alboran Basin: insights from Leg 161 results. *Proc. Ocean Drilling Program, Sci. Results* **161**, 555-580.

COOK, N.J. & CHRYSSOULIS, S.L. (1990): Concentrations of "invisible gold" in the common sulfides. *Can. Mineral.* **28**, 1-16.

DEMOUSTIER, A., CASTROVIEJO, R. & CHARLET, J.M. (1998): Clasificación textural del cuarzo epitermal (Au–Ag) de relleno filoniano del area volcánica de Cabo de Gata, Almería. *Bol. Geol. Min.* **109**, 29-48.

DEWEY, J.F. (1988): Extensional collapse of orogens. *Tectonics* **7**, 1123-1139.

DI BATTISTINI, G., TOSCANI, L., IACCARINO, S. & VILLA, I.M. (1987): K/Ar ages and the geological setting of calc-alkaline volcanics rocks from Sierra de Gata, SE Spain. *Neues Jahrb. Mineral., Monatsh.*, 369-383.

EGELER, C.G. & SIMON, O.J. (1969): Orogenic evolution of the Betic zone (Betic Cordilleras, Spain), with emphasis on the nappe structures. *Geol. Mijnb.* **48**, 296-305.

FERNÁNDEZ SOLER, J.M. (1996): *El vulcanismo calco-alcalino en el Parque Natural de Cabo de Gata – Nijar (Almeria). Estudio volcanológico y petrológico.* Ph.D. thesis, Univ. de Granada, Granada, Spain; Soc. Almeriense Historia Natural.

FLEET, M.E. & MUMIN, A.H. (1997): Gold-bearing arsenian pyrite and marcasite and arsenopyrite from Carlin Trend gold deposits and laboratory synthesis. *Am. Mineral.* **82**, 182-193.

GAMMONS, C.H. & BARNES, H.L. (1989): The solubility of Ag$_2$S in near-neutral aqueous sulfide solutions at 25 to 300°C. *Geochim. Cosmochim. Acta* **53**, 279-290.

_____ & WILLIAMS-JONES, A.E. (1995): Hydrothermal geochemistry of electrum. Thermodynamic constraints. *Econ. Geol.* **90**, 420-432.

GARCÍA DUEÑAS, V., BALANYA, J.C. & MARTINEZ, J.M. (1992): Miocene extensional detachments in the outcropping basements of the northern Alboran Basin (Betics). *Geomarine Lett.* **12**, 88-95.

HEALEY, R.E. & PETRUK, W. (1990): Petrology of Au–Ag–Hg alloy and "invisible" gold in the Trout Lake massive sulfide deposit, Flin Flon, Manitoba. *Can. Mineral.* **28**, 189-206.

HERNANDEZ, J. & BELLON, H. (1985): Chronologie K–Ar du volcanisme miocène du Rif Oriental (Maroc): implications tectoniques et magmatologiques. *Rev. Géol. Dynam. et Géogr. Phys.* **26**, 85-94.

HONG HANLIE (2000): Behaviour of gold in the weathered mantle at Shewushan, Hubei, China. *J. Geochem. Explor.* **68**, 57-68.

HYLAND, M.M. & BANCROFT, G.M. (1989): An XPS study of gold deposition at low temperatures on sulphide minerals: reducing agents. *Geochim. Cosmochim. Acta* **53**, 367-372.

JEAN, G.E. & BANCROFT, G.M. (1985): An XPS and SEM study of gold deposition at low temperature on sulphide mineral surfaces: concentration of gold by adsorption/reduction. *Geochim. Cosmochim. Acta* **49**, 979-987.

KNIPE, S.W., FOSTER, R.P. & STANLEY, C.J. (1992): Role of sulphide surfaces in sorption of precious metals from hydrothermal fluids. *Trans. Inst. Mining Metall.* **B101**, 83-88.

KOJONEN, K. & JOHANSON, B. (1999): Determination of refractory gold distribution by microanalysis, diagnostic leaching and image analysis. *Mineral. Petrol.* **67**, 1-19.

KRUPP, R.E. & WEISER, T. (1992): On the stability of gold–silver alloys in the weathering environment. *Mineral. Deposita* **27**, 268-275.

KUCHA, H., STUMPFL, E.E., PLIMER, I.R. & KÖCK, R. (1994): Gold–pyrite association – result of oxysulphide and polysulphide transport of gold? *Trans. Inst. Mining Metall.* **B103**, 197-205.

LÓPEZ RUIZ, J. & RODRÍGUEZ BADIOLA, E. (1980): La región volcánica del sureste de España. *Estudios Geológicos* **36**, 5-63.

MOLLER, P. & KERSTEN, G. (1994): Electrochemical accumulation of visible gold on pyrite and arsenopyrite surfaces. *Mineral. Deposita* **29**, 404-413.

MORALES, S. (1994): *Mineralogía, geoquímica y metalogenia de los yacimientos hidrotermales del SE de España.* Ph.D. thesis, Universidad de Granada, Granada, Spain.

MORALES RUANO, S., CARRILLO ROSÚA, F.J., FENOLL HACH-ALÍ, P., DE LA FUENTE CHACÓN, F. & CONTRERAS LÓPEZ, E. (1999): The Au–Cu epithermal deposit at Palai–Islica, Almeria, SE of Spain: preliminary data. *In* Mineral Deposits: Processes to Processing (C.J. Stanley *et al.*, eds.). Balkema, Rotterdam, The Netherlands (59-62).

_____, _____, _____, _____ & _____ (2000): Epithermal Cu–Au mineralization in the Palai–Islica deposit, Almeria, southeastern Spain: fluid-inclusion evidence for mixing of fluids as a guide to gold mineralization. *Can. Mineral.* **38**, 553-565.

MORRISON, G.W., ROSE, W.J. & JAIRETH, S. (1991): Geological and geochemical controls on the silver content (fineness) of gold in gold–silver deposits. *Ore Geol. Rev.* **6**, 333-364.

PINEDA VELASCO, A. (1984): Las mineralizaciones metálicas y su contexto geológico en el área volcánica Neógena del Cabo de Gata (Almería, SE de España). *Bol. Geol. Min.* **95**, 569-592.

RENDERS, P.J. & SEWARD, T.M. (1989): The adsorption of thio-gold (I) complexes by amorphous As$_2$S$_3$ and Sb$_2$S$_3$ at 25 and 90°C. *Geochim. Cosmochim. Acta* **53**, 255-267.

SAUNDERS, J.A. (1994): Silica and gold textures in bonanza ores of the Slepper deposit, Humboldt County, Nevada: evidence for colloids and implications for epithermal ore-forming processes. *Econ. Geol.* **89**, 628-638.

SCAINI, M.J., BANCROFT, G.M. & KNIPE, S.W. (1996): An XPS, AES and SEM study of the interactions of gold and silver chloride species with PbS and FeS_2: comparison to natural samples. *Geochim. Cosmochim. Acta* **61**, 1223-1231.

SCHOONEN, M.M.A., FISHER, N.S. & WENTE, M. (1992): Gold sorption onto pyrite and goethite: a radiotracer study. *Geochim. Cosmochim. Acta* **56**, 1801-1814.

SCOTNEY, P., BURGESS, R. & RUTTER, E.H. (2000): $^{40}Ar/^{39}Ar$ age of the Cabo de Gata volcanic series and displacements on the Carboneras fault zone, SE Spain. *J. Geol. Soc. London* **157**, 1003-1008.

SEWARD, T.M. & BARNES, H.L. (1997): Metal transport by hydrothemal ore fluids. *In* Geochemistry of Hydrothermal Ore Deposits (H.L. Barnes, ed.; 3rd edition). John Wiley & Sons, New York, N.Y. (435-486).

SHIKAZONO, N. & SHIMIZU, M. (1987): The Ag/Au ratio of native gold and electrum and the geochemical environment of gold vein deposits in Japan. *Mineral. Deposita* **22**, 309-314.

STARLING, A., GILLIGAN, J.M., CARTER, A.H.C. FOSTER, R.P. & SAUNDERS, R.A. (1989): High temperature hydrothermal precipitation of precious metals on the surface of pyrite. *Nature* **340**, 298-300.

ZECK, H.P., MONIÉ, P., VILLA, I.M. & HANSEN, B.T. (1992): Very high rates of cooling and uplift in the Alpine belt of the Betic Cordilleras, southern Spain. *Geology* **20**, 79-82.